

Article

Study on Performance of Concentric Threshing Device with Multi-Threshing Gaps for Rice Combines

Yanbin Liu, Yaoming Li *, Lipeng Chen, Tao Zhang, Zhenwei Liang , Mingsen Huang and Zhan Su

Key Laboratory of Modern Agricultural Equipment and Technology, Ministry of Education, Jiangsu University, Zhenjiang 212013, China; 2111916005@stmail.ujs.edu.cn (Y.L.); 2211816026@stmail.ujs.edu.cn (L.C.); 2111816014@stmail.ujs.edu.cn (T.Z.); zhenwei_liang@ujs.edu.cn (Z.L.); 2111716002@stmail.ujs.edu.cn (M.H.); 2111916011@stmail.ujs.edu.cn (Z.S.)

* Correspondence: ymli@ujs.edu.cn

Abstract: S concentric threshing device can improve rice crop separation and transportation capabilities. As one of the main factors affecting the threshing performance of rice combine harvesters, the threshing gap can influence the grain unthreshed rate and the grain damage rate directly. However, the clearance between any threshing cylinder tooth and the concave grid is constant for the traditional threshing device, named the single threshing gap in this paper, resulting in a consistently high total loss rate (the sum of unthreshed and damaged grains). Therefore, multi-threshing gaps are proposed in this paper for the concentric threshing device to solve the above problem. To compare the threshing performance between the single threshing gap and the multi-threshing gaps, the movement process of rice mixture (grain, short straw, and long straw) was simulated using the discrete element method (DEM). The simulation results showed that the separation and transportation abilities of the multi-threshing gaps were not decreased, but the distribution of threshed output mixture was more even for the multi-threshing gaps. Furthermore, a field experiment was also carried out on a combine harvester to compare the total loss rate. The experiment results showed that the total loss rate of the concentric threshing device with multi-threshing gaps was reduced by 0.0593%, which was 5.77% less than the total loss rate of the concentric threshing device with a single threshing gap.

Keywords: rice threshing; concentric threshing device with multi-threshing gaps; discrete element method; grain unthreshed rate; grain damage rate



Citation: Liu, Y.; Li, Y.; Chen, L.; Zhang, T.; Liang, Z.; Huang, M.; Su, Z. Study on Performance of Concentric Threshing Device with Multi-Threshing Gaps for Rice Combines. *Agriculture* **2021**, *11*, 1000. <https://doi.org/10.3390/agriculture11101000>

Academic Editors: Riccardo Testa, Giuseppina Migliore, Giorgio Schifani and József Tóth

Received: 29 August 2021
Accepted: 11 October 2021
Published: 13 October 2021

Publisher's Note: MDPI stays neutral with regard to jurisdictional claims in published maps and institutional affiliations.



Copyright: © 2021 by the authors. Licensee MDPI, Basel, Switzerland. This article is an open access article distributed under the terms and conditions of the Creative Commons Attribution (CC BY) license (<https://creativecommons.org/licenses/by/4.0/>).

1. Introduction

Rice is an important cereal crop and provides energy and nutrition for about half of the world's population owing to its high starch content [1,2]. Combine harvesters are critical in rice harvesting, and the threshing performance of threshing device plays a key role in the whole harvest process [3]. Threshing gap is the clearance between the threshing cylinder tooth and the concave grid, which is one of the main factors affecting threshing performance [4]. Adjusting the threshing gap using a concentric threshing device changes the diameter of the threshing cylinder by adjusting the elongation of the threshing rods [5]. Su et al. [6] proved that the threshing performances (the transportation and separation capacities, the distribution of the threshed output mixture) of a concentric threshing device were superior. Strong conveying and separation abilities can effectively prevent the blockage of the threshing device, and the distribution of the threshed output mixture will affect the performance of the cleaning device [7].

Several studies have been carried out on the effect of the threshing gap on the threshing performance. It was proven that the grain unthreshed rate was increased and the grain damage decreased with the increment in the threshing gap [8–11]. This was because of the decrease in threshing force on the material in the added moving space [12,13]. To be specific, the clearance between any one of the threshing cylinder teeth and the concave grid is the same (single threshing gap), which means the material is continually subjected

to either too much or too little threshing force throughout the threshing process, which results in a contradictory relationship between the grain unthreshed rate and the grain damage rate; thus, the total loss rate (the sum of unthreshed and damaged grains) stays at a high level.

Therefore, multi-threshing gaps are proposed in this paper for the concentric threshing device to solve the above problem. Furthermore, the transportation capacity and the distribution of the threshed output mixture of the concentric threshing device with multi-threshing gaps also need to be studied. However, the movement process of material in a threshing device is very complicated, and it is difficult to intuitively obtain the movement state of material in a threshing device using traditional research methods [11,14]. With the rapid development in computational technology, the discrete element method (DEM) has been widely used in agricultural engineering, such as tillage [15], manure spreading [16,17], and seeding [18,19]. For the agricultural harvest process, Coetzee et al. [20] developed a DEM model of a bunch of grapes and a DEM model of a commercial destemmer, which could accurately simulate the amount of berries removed from stems, the quantity of impurities mixed with the berries at the discharge, and the spatial distribution of berries. Ma et al. [21] simulated the motion process of grain and straw in a 3-DOF variable-amplitude screen box using DEM, and the results showed that the agricultural particles at the screen front were thrown up and moved back much more quickly, but the separation of different materials was not improved. Yu et al. [22] validated the feasibility and effectiveness of DEM through comparing the numerical results with experimental data in analyzing the corn threshing process. Liang et al. [23] established rice grain and short straw particle models according to their physical properties, and discrete element method (DEM) simulations were carried out to understand their collision behavior with the grain loss sensor. Romuli et al. [24] used DEM to simulate the hulling process of *Jatropha curcas* L. fruits. Moreover, Su et al. [6] verified that the DEM could accurately simulate the movement of rice mixture (grains, short straw, and long straw) in a threshing device. However, it is very difficult to use DEM to simulate the actual rice threshing process to measure the grain unthreshed rate and the grain damage rate.

Considering the current research progress, the performance of concentric threshing device with multi-threshing gaps was studied in this paper.

2. Materials and Methods

2.1. Establishment of Models of Concentric Threshing Device with Single and Multi-Threshing Gaps

According to the longitudinal axial flow threshing device of a YANMAR-AW82G combine harvester (YANMAR, Osaka, Japan) (see Figure 1), three combinations of threshing rod elongation were put forward. The threshing rods were named 1–6 in the clockwise direction, as shown in Figure 2. The combination method of the threshing rod elongation is shown in Table 1.

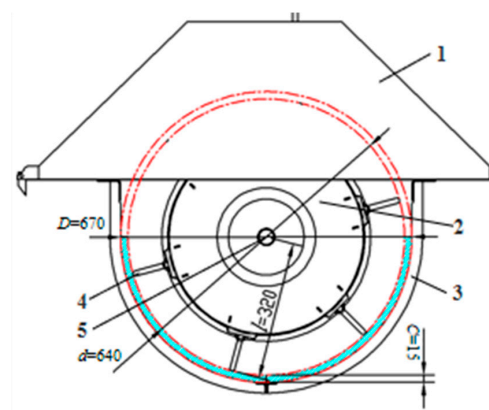


Figure 1. Schematic diagram of the threshing device of YANMAR-AW82G combine harvester: 1—top cover; 2—threshing cylinder; 3—concave grid; 4—threshing cylinder tooth; 5—shaft; D and d are the

diameters of the concave grid and threshing cylinder respectively, mm; C is the threshing gap, mm; l is the elongation of threshing rod (distance between the outer end of the threshing cylinder teeth and the center of the shaft), mm.

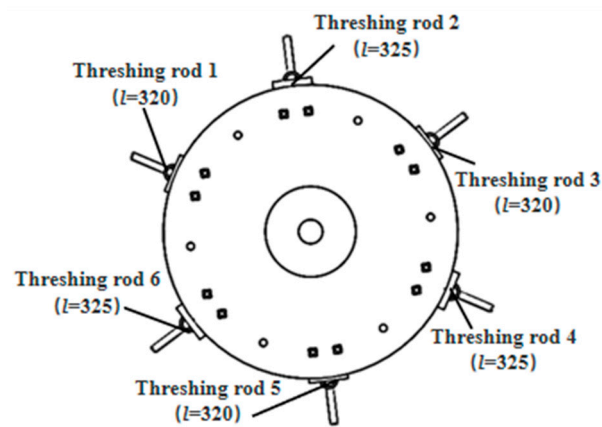


Figure 2. Schematic diagram of the multi-threshing gaps and the threshing rods 1–6.

Table 1. Combination method of the threshing rod elongation.

No. l , mm	Threshing Rod 1	Threshing Rod 2	Threshing Rod 3	Threshing Rod 4	Threshing Rod 5	Threshing Rod 6
1	320	320	320	320	320	320
2	325	325	325	325	325	325
3	320	325	320	325	320	325

From Table 1, the threshing gaps of the first and second combinations characterized concentric threshing devices with a single threshing gap of 15 mm and 10 mm, respectively. The third combination method was a concentric threshing device with multi-threshing gaps, whereby the threshing gap of threshing rods 1, 3, and 5 was 15 mm, and the threshing gap of threshing rods 2, 4, and 6 was 10 mm, as shown in Figure 2.

2.2. Simulation Model Building

2.2.1. Concentric Threshing Device

A 3D model of the concentric threshing device was modeled and simplified in SolidWorks (v.2020, Dassault Systèmes, Vélizy-Villacoublay, France) referring to the YANMAR-AW82G combine harvester, before being saved in Step format and imported into EDEM 2020. The simulation model of the concentric threshing device is shown in Figure 3, which was mainly composed of the top cover, threshing cylinder (three threshing cylinders were built according to Table 1), guard plate, concave grid, and 16 reception boxes. The material of the threshing device was set as steel, and the parameters are shown in Table 2.

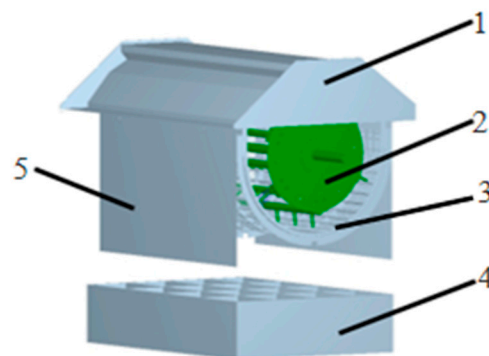


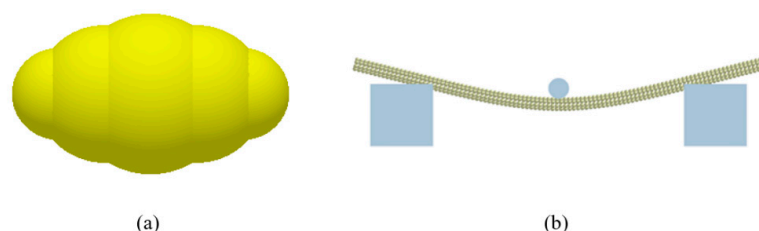
Figure 3. Schematic diagram of simulation model of threshing device: 1—top cover; 2—threshing cylinder; 3—concave grid; 4—reception box; 5—guard plate.

Table 2. Material parameters setting in the DEM simulation [6].

Simulation Material	Poisson's Ratio	Elastic Modulus E, MPa	Density, kg/m ³
Rice grain	0.28	375	1350
Rice straw	0.4	2.8	215
Steel	0.3	2.06×10^5	7800

2.2.2. Rice Mixture

The establishment of a rice plant model in the simulation process can greatly increase the simulation time [11]. The rice mixture in the threshing process mainly includes grains, short straw, and long straw. Therefore, only rice grains and short straw with a length of 50 mm and long straw with a length of 150 mm were considered in the simulation process to improve the accuracy and efficiency of the simulation. A flexible rice straw was established, which could bend, deform, or even break under the stress state. The discrete element model of rice grain and flexible straw established by Su et al. [6] was adopted in this simulation, as shown in Figure 4. The material parameters are shown in Table 2, and the bonding parameters of the flexible straw model are shown in Table 3.

**Figure 4.** DEM model of rice grain (a) and flexible rice straw (b).**Table 3.** Bonding parameters of the flexible rice straw [6].

Bonding Parameters	Values
Bonded disk radius, mm	2.11
Normal bonding stiffness, N/m ³	2.35×10^9
Tangential bonding stiffness, N/m ³	7.91×10^9
Bonding parameters	Values

2.3. Simulation Design

The rotational speed of the threshing cylinder was set to 570 rpm according to the YANMAR-AW82G combine (YANMAR, Osaka, Japan). According to the physical properties of "Wuyun Keng 24" rice, the number of grains per ear was about 125. The length of the rice straw was about 500 mm, excluding the ear length and the height of remaining stubble, which could be roughly divided into 5 short straw and 1.6 long straw. Therefore, the quantity percentage of grains, short straw, and long straw was 625:25:8. The particle factory produced 5600 grains, 225 short straws, and 70 long straws per second at the feeding end of the threshing device. The particle generation time was set to 1 s, and the total simulation time was 3 s. Contact parameters among the rice grains, straw, and threshing device are shown in Table 4. By only changing the simulation model of the threshing cylinder, the movement of the rice mixture in the threshing device and the distribution of the threshed output mixture in the reception box using a concentric threshing device with three different threshing gaps were simulated.

Table 4. Contact parameters between various materials [6].

Contact Parameter	Restitution Coefficient	Static Friction Coefficient	Rolling Friction Coefficient
Rice grain–rice grain	0.5	0.425	0.01
Rice grain–rice straw	0.2	0.8	0.01
Rice grain–steel	0.5	0.58	0.01
Rice straw–rice straw	0.2	0.9	0.01
Rice straw–steel	0.2	0.8	0.01

2.4. Field Experiment

2.4.1. Experimental Device

To facilitate the adjustment of three threshing gaps, a longitudinal axial-flow threshing cylinder was designed, which could independently adjust the elongation of each threshing rod; it was adopted in this study to provide the device basis for field experiments. It was processed in Suzhou Jiufu Agricultural Machinery Co., Ltd. (Suzhou, China) and mounted on the YANMAR-AW82G rice combine harvester (YANMAR, Osaka, Japan), as shown in Figure 5.



Figure 5. Threshing device for individually adjusting threshing rod elongation.

Working principle (see Figure 6): When the elongation of threshing rod needs to be adjusted, the DC motor rotates in a positive and negative direction, driving the worm and worm wheel reducer. The worm and worm wheel reducer have two output shafts; the upper output shaft drives the correcting element 1, and the lower output shaft moves the synchronous transmission device to synchronously transmit the power to the correcting elements 2 and 3. Then, the three correcting elements of the same mechanism principle synchronously drive the threshing rod radial movement up and down. Each correcting element is composed of a transmission shaft, a screw, and a jaw. The transmission shaft drives the screw to rotate so as to move the jaw to move up and down. The jaw is connected with the threshing rod, and the transmission shafts are connected with the output shaft of the worm and worm wheel reducer and the synchronous transmission device.

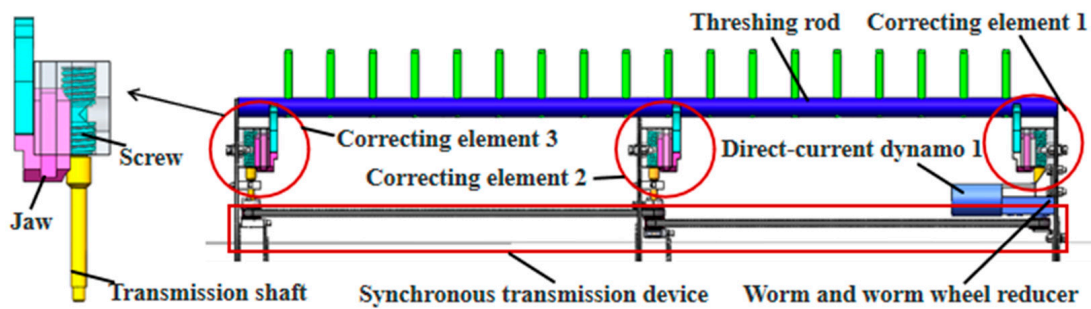


Figure 6. Schematic diagram of working principle.

2.4.2. Experimental Method and Indices

The test location was the Wujiang District test field (Suzhou, China). The rice variety was “Jia Hua”, and its physical properties are shown in Table 5. Before the experiment, rice fields with basically the same crop growth were selected as the experiment area. During the experiment, the length of the experiment area for each test group was 20×2.06 m, and each test group underwent three parallel tests, where the average value was taken. The threshing performance indices of threshing device were the grain unthreshed rate, the grain damage rate, and the total loss rate (the sum of unthreshed and damaged grains). After the end of each parallel test, the material discharged from the tail of threshing cylinder collected by the tarpaulin attached to the tail of threshing cylinder was used to calculate the grain unthreshed rate, and the grain damage rate was calculated by randomly selecting grain samples in the grain tank [25].

Table 5. Physical properties of “Jia Hua” rice.

Parameters	Values
Plant height (mm)	792
Ear length (mm)	161
Grain moisture content (%)	20.6
Straw moisture content (%)	70.8
Straw/grain ratio	2.25
Number of grains per ear	135
Thousand-seed mass (g)	32.4

The grain unthreshed rate, the grain damage rate, and the total loss rate were respectively calculated using Equations (1)–(3).

$$Y_T = \frac{W_T}{W_M} \times 100\%, \quad (1)$$

where Y_T is the grain un-threshed rate (%), W_T is the grain weight remaining on the ear discharged from the end of threshing cylinder (g), and W_M is the total weight of grains (g).

$$Y_C = \frac{W_C}{W_S} \times 100\%, \quad (2)$$

where Y_C is the grain damage rate (%), W_T is the weight of damaged grains in the sample (g), and W_S is the total weight of grains in the sample (g).

$$Y = Y_T + Y_C, \quad (3)$$

where Y is the total loss rate (%).

2.4.3. Experimental Design

Three levels of threshing gap for the concentric threshing device were selected: a single threshing gap of 10 mm (A), a single threshing gap of 15 mm (B), and multi-threshing gaps of 10 mm and 15 mm (C). By changing the forward speed of the combine harvester to change the feeding rate, there were three levels of forward speed: 0.8 m/s, 1.0 m/s, and 1.2 m/s. A total of nine groups of tests were carried out. The experimental design is shown in Table 6.

Table 6. Experimental design.

No.	Forward Speed, m/s	Feeding Rate, kg/s	Threshing Gap, mm
1	0.8	3.6	A
2	0.8	3.6	B
3	0.8	3.6	C
4	1.0	4.5	A
5	1.0	4.5	B
6	1.0	4.5	C
7	1.2	5.4	A
8	1.2	5.4	B
9	1.2	5.4	C

3. Results and Discussion

3.1. Analysis of Simulation Results

3.1.1. The Circumferential Distribution of Rice Mixture

After the simulation was completed, the analysis module of EDEM was used to set the rice grain as green, long straw as blue, and short straw as red. When the simulation time was 0.5 s and 1 s, the circumferential distribution of the rice mixture in the concentric threshing device was analyzed, as shown in Figures 7 and 8.

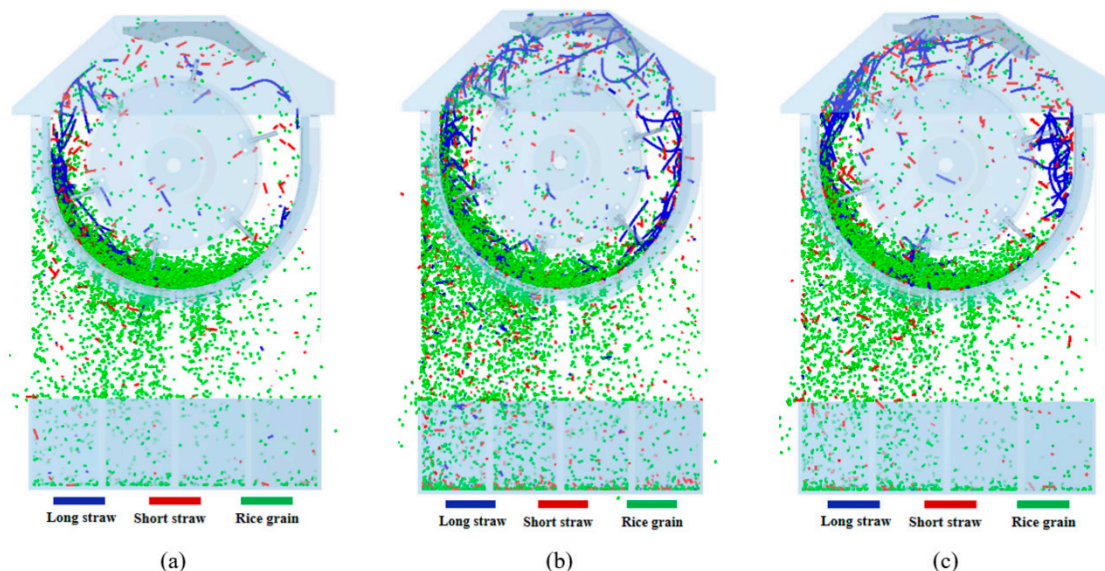


Figure 7. Circumferential distribution of rice mixture in the concentric threshing device at 0.5 s: (a) single threshing gap of 15 mm; (b) single threshing gap of 10 mm; (c) multi-threshing gaps of 10 mm and 15 mm.

At 0.5 s, in the simulation model of the single threshing gap of 15 mm, the mixture was mainly concentrated in the lower left part of the threshing device, because the larger threshing gap had a weaker stirring ability to the crop and the rotating direction of threshing cylinder, as shown in Figure 7a. The simulation model of the single threshing gap of 10 mm is shown in Figure 7b, where the circumferential distribution of mixture was significantly more uniform because threshing cylinder teeth had a stronger stirring ability toward

materials in the smaller threshing gap, and it was easier to drive materials to rotate along with the threshing cylinder. However, more blue and red materials passed through the concave grid, indicating that the threshing cylinder teeth had a stronger impact on materials under the smaller threshing gap to break more rice flexible straw. To some extent, this indicated that the grain damage rate would increase with the decrease in the threshing gap. The simulation model of the multi-threshing gaps of 10 mm and 15 mm is shown in Figure 7c, where the circumferential distribution of mixture was uniform, and the blue and red materials under the concave grid were significantly less prevalent than in the simulation model of the single threshing gap of 10 mm.

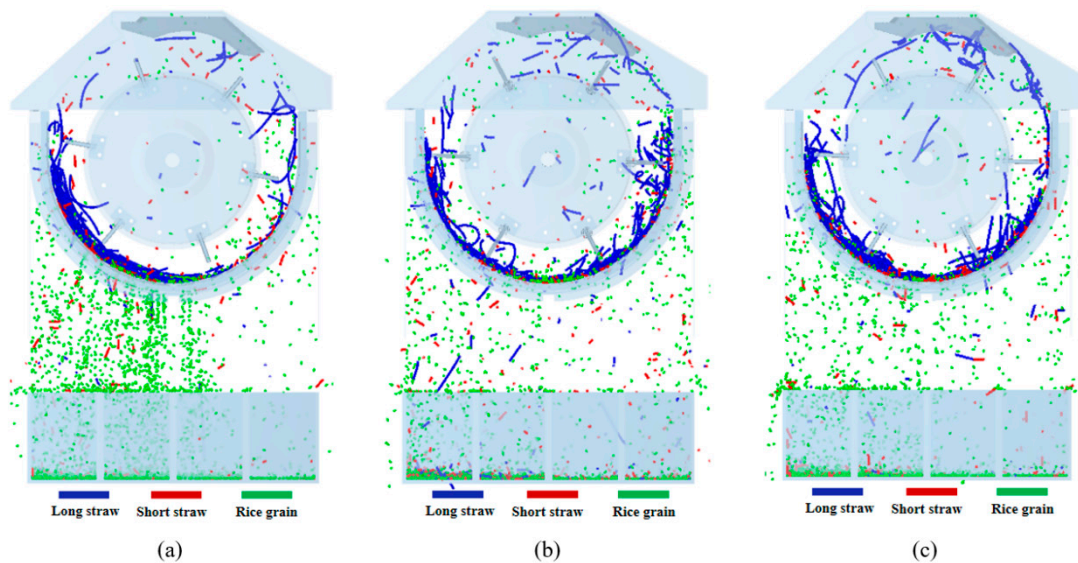


Figure 8. Circumferential distribution of rice mixture in the concentric threshing device at 1 s: (a) single threshing gap of 15 mm; (b) single threshing gap of 10 mm; (c) multi-threshing gaps of 10 mm and 15 mm.

At 1 s, the simulation model of the single threshing gap of 15 mm is shown in Figure 8a, where a large amount of straw was still mainly concentrated in the lower left part of the threshing device, and several grains did not fall into the reception box. In the simulation model of the single threshing gap of 10 mm and multi-threshing gaps of 10 mm and 15 mm, most grains passed through the concave grid into the reception box, and the mixture was still uniformly distributed in the circumferential direction, as shown in Figure 8b,c. Nevertheless, in the simulation model of the single threshing gap of 10 mm, the blue and red materials under the concave grid were still most prevalent.

In conclusion, the material distribution along the circumferential direction was even and the separation capacity was strong in the model with multi-threshing gaps of 10 mm and 15 mm, being similar to the model with the single threshing gap of 10 mm. To some extent, the multi-threshing gaps did not affect the conveying and separation capacities of the concentric threshing device.

3.1.2. Variation in Total Quantity and Average Velocity of Rice Mixture

To accurately analyze the changes in the total amount and average velocity of rice mixture in the concentric threshing device, grid bin group 1 was established in EDEM, as shown in Figure 9. The cell size was $200 \times 158 \times 160$ mm, and the fixed time step was 20%. The range of grid bin group 1 included the entire upper side of the concave grid and all areas between the feed inlet and the discharge outlet of the threshing device.

As shown in Figure 10, the maximum value of the total amount of mixture was the smallest in the simulation model of the single threshing gap of 10 mm, which was mainly because the threshing cylinder teeth had the strongest threshing ability toward the material, resulting in more discrete element models of rice flexible straw being broken. Subsequently, the broken straw along with the grains passed through the concave grid. Since the multi-

threshing gaps of 10 mm and 15 mm were relative to the single threshing gap of 15 mm with better grain screening capacity, this resulted in more grains through the concave grid into the reception box ahead of time; thus, the peak value of the total quantity of mixture was the second lowest. After the peak value, the total amount of mixture dropped sharply. In the simulation models of the single threshing gap of 10 mm and multi-threshing gaps of 10 mm and 15 mm, the variation trend of the total quantity was consistent and tended to be stable at around 1.65 s. The total amount of mixture of the single threshing gap of 15 mm stabilized at about 1.75 s, and the total amount of mixture was the largest. The results showed that the single threshing gap of 10 mm and the multi-threshing gaps of 10 mm and 15 mm both had a similarly stronger conveying and screening capacity than the single threshing gap of 15 mm.

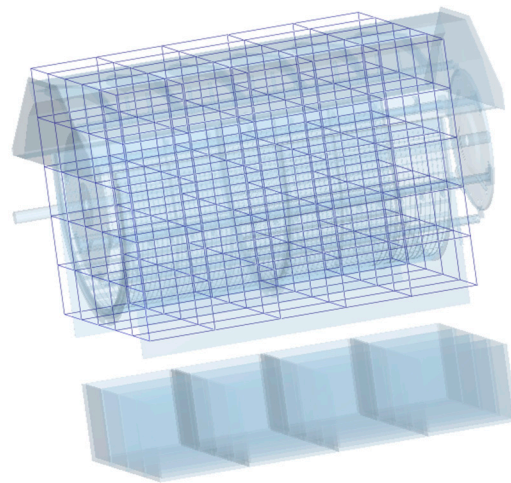


Figure 9. Grid bin group 1.

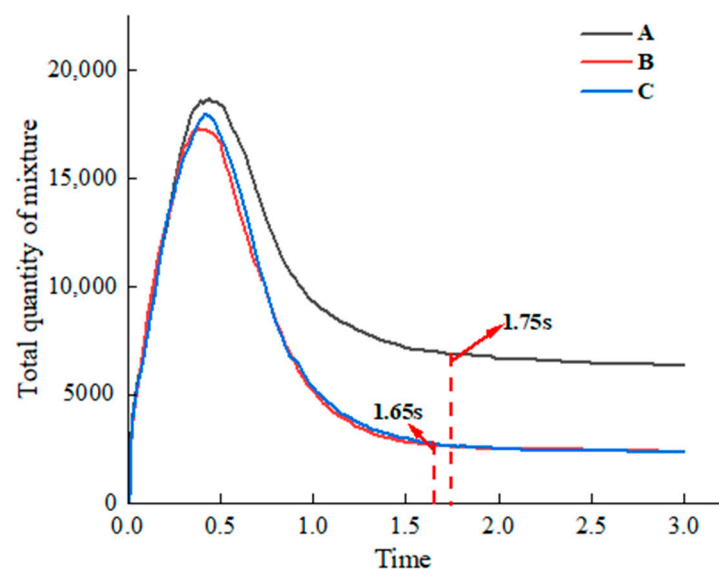


Figure 10. The relationship between the total quantity of mixture in the concentric threshing device and time: (A) single threshing gap of 15 mm; (B) single threshing gap of 10 mm; (C) multi-threshing gaps of 10 mm and 15 mm.

As shown in Figure 11, the average velocities of mixture in three simulation models were basically the same at the beginning. At 0.1 s, the average velocity curve declined sharply because the number of collisions between the mixture and threshing cylinder teeth in the threshing device increased. The average velocities of the mixtures in the models of the single threshing gap of 10 mm and multi-threshing gaps of 10 mm and

15 mm varied similarly. However, after 1.3 s, the average velocity of the mixture in the model with multi-threshing gaps of 10 mm and 15 mm was slightly higher. The average velocity of the mixture in the model with the single threshing gap of 15 mm dropped the fastest and was the lowest. This was due to the single threshing gap of 10 mm and multi-threshing gaps of 10 mm and 15 mm having a stronger agitating ability toward the material, whereby the material had better flow in the threshing device. It was indicated again that the multi-threshing gaps did not affect the conveying capacity of the threshing device and the screening capacity of the concave grid.

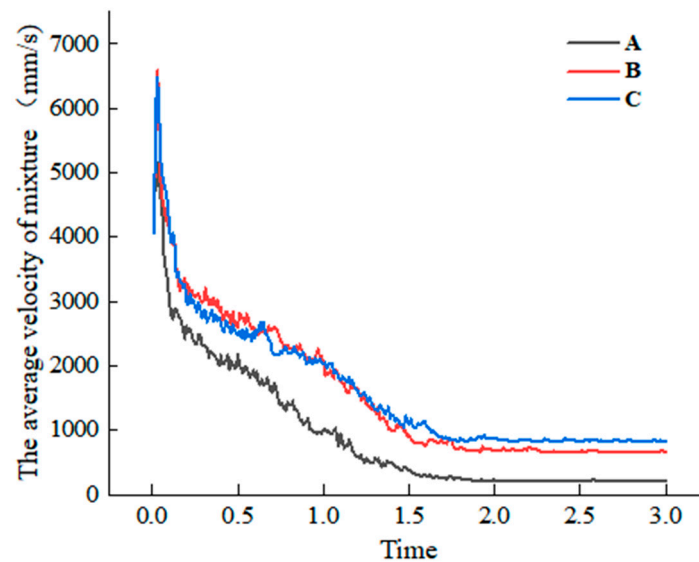


Figure 11. The relationship between the average velocity of mixture in the concentric threshing device and time: (A) single threshing gap of 15 mm; (B) single threshing gap of 10 mm; (C) multi-threshing gaps of 10 mm and 15 mm.

3.1.3. Distribution Status of the Threshed Output Mixture

To accurately analyze the distribution status of the threshed output mixture in reception boxes, grid bin group 2 was built in EDEM, as shown in Figure 12. The percentage quantity distributions of the threshed output mixture in the 16 receiving boxes in the three simulation models were exported, as shown in Figure 13.

In Figures 12 and 13, the X-axis is the axial direction of threshing device, and the Y-axis is the radial direction of threshing device. Figure 13 shows that the percentage decreased with the increase in X-axis and increased with the increase in Y-axis. In the three simulation models, most of the threshed output mixture was concentrated in the upper right corner owing to the rotation direction of the threshing cylinder, and because most of the grains fell at the feeding inlet end of the threshing device.

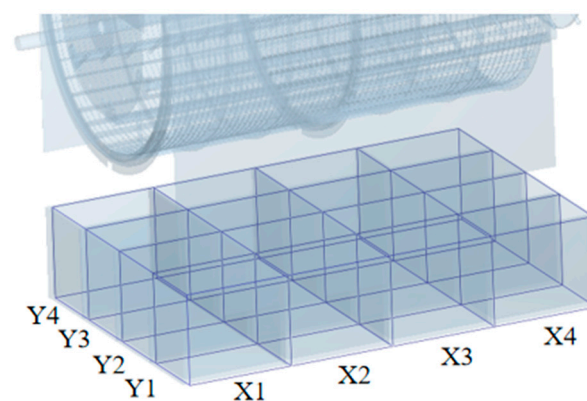


Figure 12. Grid bin group 2.

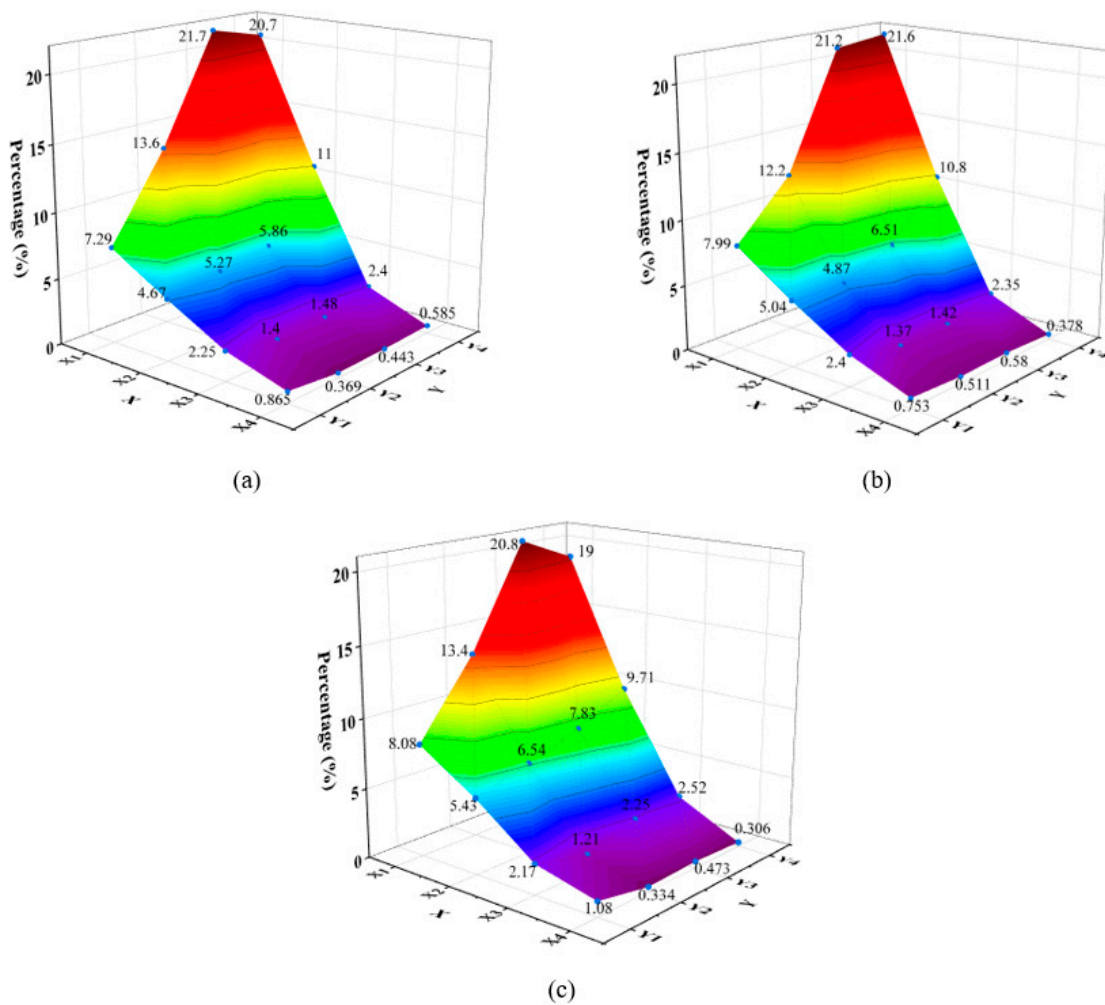


Figure 13. Percentage quantity distributions of the threshed output mixture in reception boxes: (a) single threshing gap of 15 mm; (b) single threshing gap of 10 mm; (c) multi-threshing gaps of 10 mm and 15 mm.

Standard deviation (SD) is most commonly used in probability statistics as a measure of the degree of statistical distribution [26,27]. Consequently, in order to accurately compare the distribution uniformity of the threshed output mixture under different threshing clearances, SD analysis was carried out for the percentage quantity distributions of the threshed output mixture in the reception boxes along the Y-axis on coordinates X1, X2, X3, and X4, in the reception boxes along the X-axis on coordinates Y1, Y2, Y3, and Y4, and in all 16 reception boxes. Since the mean of each dataset was different, the standard deviation coefficient (SDC) needed to be calculated. A smaller SDC denotes a more uniform distribution. The mean, SD, and SDC are shown in Tables 7 and 8.

Table 7. Statistical table of the mean (M), standard deviation (SD), and standard deviation coefficients (SDC) of percentage distributions along the Y-axis on coordinates X1, X2, X3, and X4: (A) single threshing gap of 15 mm; (B) single threshing gap of 10 mm; (C) multi-threshing gaps of 10 mm and 15 mm.

Model	Item	X1 (Y)	X2 (Y)	X3 (Y)	X4 (Y)
A	M ± SD	15.8456 ± 6.7516	6.707 ± 2.9211	1.882 ± 0.5143	0.5655 ± 0.2191
	SDC	42.61%	43.55%	27.33%	38.74%
B	M ± SD	15.7483 ± 6.7529	6.8144 ± 2.7786	1.8859 ± 0.5675	0.556 ± 0.1560
	SDC	42.89%	40.77%	30.09%	28.06%
C	M ± SD	15.3112 ± 5.7408	7.3771 ± 1.8384	2.0375 ± 0.5687	0.5492 ± 0.3643
	SDC	37.49%	24.92%	27.91%	66.33%

Table 8. Statistical table of the mean (M), standard deviation (SD), and standard deviation coefficients (SDC) of percentage distributions along the X-axis on coordinates Y1, Y2, Y3, and Y4: (A) single threshing gap of 15 mm; (B) single threshing gap of 10 mm; (C) multi-threshing gaps of 10 mm and 15 mm.

Model	Item	Y1 (X)	Y2 (X)	Y3 (X)	Y4 (X)	All
A	M ± SD	3.768 ± 2.8267	5.1652 ± 6.0181	7.3787 ± 9.8535	8.6881 ± 9.2354	6.25 ± 7.0143
	SDC	75.02%	116.51%	133.54%	106.30%	112.23%
B	M ± SD	4.0457 ± 3.1655	4.7359 ± 5.318	7.4219 ± 9.5334	8.7965 ± 9.6796	6.25 ± 6.9670
	SDC	78.24%	112.29%	128.45%	110.04%	111.47%
C	M ± SD	4.1931 ± 3.1833	5.3775 ± 6.0256	7.8259 ± 9.1694	7.8785 ± 8.4221	6.25 ± 6.5564
	SDC	75.92%	112.05%	117.17%	106.90%	104.90%

Along the Y-axis direction (see Table 7), in the model with multi-threshing gaps of 10 mm and 15 mm, the SDC of percentage distribution on the X1 and X2 coordinates was the minimum, that on the X3 coordinate was the second smallest, and that on the X4 coordinates was the largest. The threshed output mixture was mainly concentrated in the reception boxes at the X1 and X2 coordinates, whereas the distribution uniformity along the Y-axis direction at the X4 coordinate had least influence on the cleaning performance of the cleaning device. Hence, along the Y-axis direction, the distribution of the threshed output mixture in the model with multi-threshing gaps of 10 mm and 15 mm was more even.

Along the X-axis direction (see Table 8), the SDC of percentage distribution of the models with multi-threshing gaps of 10 mm and 15 mm on the Y2 and Y3 coordinates was the minimum, and that on the Y1 and Y4 coordinates was close to the single threshing gap of 15 mm. Meanwhile, the SDC of percentage of the model with multi-threshing gaps of 10 mm and 15 mm in all 16 reception boxes was the minimum (see Table 8). Thus, along the X-axis direction and from the overall distribution, the distribution of the threshed output mixture in the model with multi-threshing gaps of 10 mm and 15 mm was also more uniform.

In summary, the threshed output mixture of the concentric threshing device with multi-threshing gaps was more evenly distributed.

3.2. Analysis of Field Experiment Results

The field experiment results are shown in Table 9 and Figure 14. With the increase in the forward speed, the grain unthreshed rate, the grain damage rate, and the total loss rate all increased. The grain unthreshed rate and the grain damage rate of the single threshing gap of 15 mm were, respectively, the highest and the lowest, and those of the single threshing gap of 10 mm were, respectively, the minimum and the maximum. The total loss rate of the two single threshing gaps were close to but significantly higher than that of the multi-threshing gaps of 10 mm and 15 mm. When the forward speed was 0.8 m/s, 1.0 m/s, and 1.2 m/s, the total loss rate of the concentric threshing device with multi-threshing gaps was respectively reduced by 0.046%, 0.048%, and 0.084%, with an average value of 0.0593%, which was 5.77% less than the total loss rate of the concentric threshing device with a single threshing gap.

Table 9. Field test results.

No.	Forward Speed, m/s	Threshing Gap, mm	Un-Threshed Rate, %	Damage Rate, %	Total Loss, %
1	0.8	A	0.262	0.42	0.682
2	0.8	B	0.173	0.5	0.673
3	0.8	C	0.177	0.45	0.627
4	1.0	A	0.511	0.51	1.021
5	1.0	B	0.425	0.61	1.035
6	1.0	C	0.433	0.54	0.973
7	1.2	A	0.856	0.58	1.436
8	1.2	B	0.657	0.79	1.447
9	1.2	C	0.732	0.62	1.352

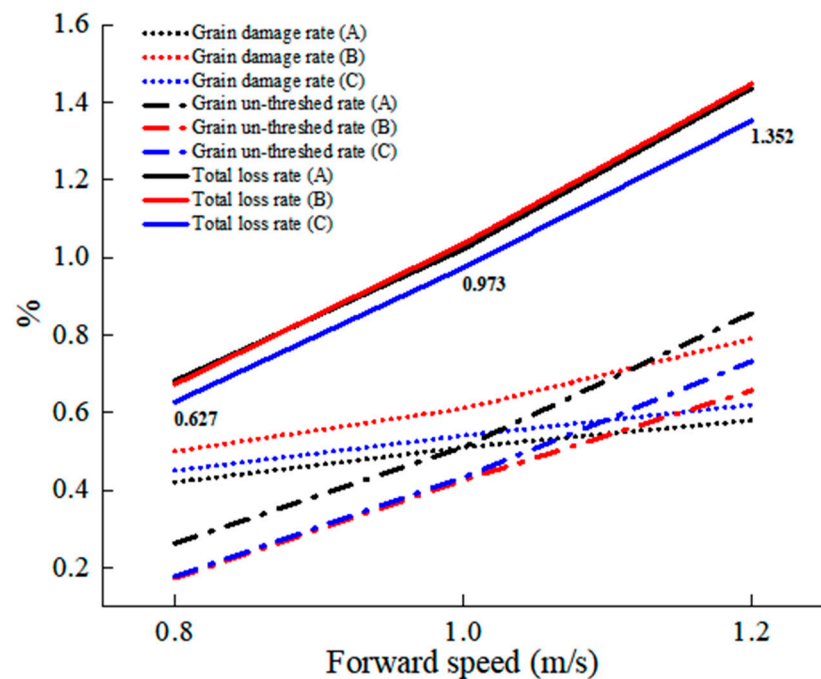


Figure 14. The relationship among the grain unthreshed rate, grain damage rate, total loss rate, and forward speed for different threshing gaps of the concentric threshing device: (A) single threshing gap of 15 mm; (B) single threshing gap of 10 mm; (C) multi-threshing gaps of 10 mm and 15 mm; the numbers denote the total loss rate of C.

4. Conclusions

The movement process of a rice mixture in a concentric threshing device with single/multi-threshing gaps was simulated using DEM. The effects of different threshing gaps on the circumferential distribution, the total quantity and average velocity of the rice mixture in the threshing device, and the distribution of the threshed output mixture in reception boxes were analyzed. Then, the influence of different threshing gaps on the grain unthreshed rate, the grain damage rate, and the total loss rate of unthreshed and damaged grains was analyzed by field experiment. The following conclusions could be drawn:

- (1) The material distribution along the circumferential direction was even and the separation capacity was strong in the simulation model of the multi-threshing gaps. Simultaneously, in the simulation model of the multi-threshing gaps, the distribution of the threshed output mixture was more uniform.
- (2) The total loss rate of the concentric threshing device with multi-threshing gaps was reduced by 0.0593%, which was 5.77% less than the total loss rate of the concentric threshing device with a single threshing gap.

However, the proposed concentric threshing device with multi-threshing gaps needs to be verified in a large number of field experiments (more than running the machine over 20 m), and feedback needs to be obtained from farmers to determine its effectiveness and practicality.

Author Contributions: Methodology, software, data curation, and writing—original draft, Y.L. (Yanbin Liu); conceptualization, funding acquisition, and validation, Y.L. (Yaoming Liu); visualization and investigation, L.C.; supervision, T.Z.; writing—review and editing, Z.L. and M.H.; DEM model of rice grain and flexible rice straw, Z.S. All authors have read and agreed to the published version of the manuscript.

Funding: The work was supported by the National Natural Science Foundation of China (No. 51975257) and the Key R&D Projects in Shandong Province of China (No. 2019JZZY010729).

Institutional Review Board Statement: Not applicable.

Informed Consent Statement: Not applicable.

Data Availability Statement: Not applicable.

Conflicts of Interest: The authors declare no conflict of interest.

References

1. Bag, M.K.; Basak, N.; Bagchi, T.; Masurkar, P.; Ray, A.; Adak, T.; Jena, M.; Rath, P.C. Consequences of *Ustilaginoidea virens* infection, causal agent of false smut disease of rice, on production and grain quality of rice. *J. Cereal Sci.* **2021**, *100*, 103220. [[CrossRef](#)]
2. Bagchi, T.B.; Chattopadhyay, K.; Sivashankari, M.; Roy, S.; Kumar, A.; Biswas, T.; Pal, S. Effect of Different Processing Technologies on Phenolic Acids, Flavonoids and Other Antioxidants Content in Pigmented Rice. *J. Cereal Sci.* **2021**, *100*, 103263. [[CrossRef](#)]
3. Liang, Z.; Li, Y.; Baerdemaeker, J.D.; Xu, L.; Saeys, W. Development and Testing of A Multi-duct Cleaning Device for Tangential-longitudinal Flow Rice Combine Harvesters. *Biosyst. Eng.* **2019**, *182*, 95–106. [[CrossRef](#)]
4. Huynh, V.; Powell, T.; Siddall, P.J. Threshing and Separating Process—A Mathematical Model. *Trans. ASAE* **1982**, *25*, 0065–0073. [[CrossRef](#)]
5. Li, Y.; Su, Z.; Liang, Z.; Li, Y. Variable-diameter Drum with Concentric Threshing Gap and Performance Comparison Experiment. *Appl. Sci.* **2020**, *10*, 5386. [[CrossRef](#)]
6. Su, Z.; Li, Y.; Dong, Y.; Tang, Z.; Liang, Z. Simulation of rice threshing performance with concentric and non-concentric threshing gaps. *Biosyst. Eng.* **2020**, *197*, 270–284. [[CrossRef](#)]
7. Chai, X.; Zhou, Y.; Xu, L.; Li, Y.; Li, Y.; Lv, L. Effect of guide strips on the distribution of threshed outputs and cleaning losses for a tangential-longitudinal flow rice combine harvester. *Biosyst. Eng.* **2020**, *198*, 223–234. [[CrossRef](#)]
8. Sewell, A.J. Some Effects of Concave to Drum Clearance and Concave Design on Small Grain Threshing Drum Performance. *J. Agric. Eng. Res.* **1990**, *46*, 207–217. [[CrossRef](#)]
9. Tang, Z.; Li, Y.; Liang, Z. Optimal Parameters Prediction and Control of Rice Threshing for Longitudinal Axial Threshing Apparatus. *Trans. Chin. Soc. Agric. Eng.* **2016**, *32*, 70–76.
10. Teng, Y.; Jin, C.; Chen, Y.; Liu, P.; Yin, X.; Wang, T.; Yu, K. Design and optimization of segmented threshing device of combine harvester for rice and wheat. *Trans. Chin. Soc. Agric. Eng.* **2020**, *36*, 1–12.
11. Wang, Q.; Mao, H.; Li, Q. Modelling and simulation of the grain threshing process based on the discrete element method. *Comput. Electron. Agric.* **2020**, *178*, 105790. [[CrossRef](#)]
12. Jin, C.; Kang, Y.; Guo, H.; Wang, T.; Yin, X. Experimental Research on the Influence of Threshing Roller Structures on the Quality of Mechanically-harvested Soybeans. *Trans. Chin. Soc. Agric. Eng.* **2021**, *37*, 49–58.
13. Li, X.; Wang, W.; Zhao, G.; Sun, C.; Hu, P.; Ji, J. Design and experiment of longitudinal axial flow double flexible rolling and kneading threshing device for millet. *Trans. Chin. Soc. Agric. Mach.* **2021**, *52*, 113–123.
14. Petkevichius, S.; Shpokas, L.; Kutzbach, H.-D. Investigation of the maize ear threshing process. *Biosyst. Eng.* **2008**, *99*, 532–539. [[CrossRef](#)]
15. Makange, N.R.; Ji, C.; Torotwa, I. Prediction of cutting forces and soil behavior with discrete element simulation. *Comput. Electron. Agric.* **2020**, *179*, 105848. [[CrossRef](#)]
16. Landry, H.; Laguë, C.; Roberge, M. Discrete element modeling of machine–manure interactions. *Comput. Electron. Agric.* **2006**, *52*, 90–106. [[CrossRef](#)]
17. Van Liedekerke, P.; Tijssens, E.; Dintwa, E.; Rioual, F.; Vangeyte, J.; Ramon, H. DEM simulations of the particle flow on a centrifugal fertilizer spreader. *Powder Technol.* **2009**, *190*, 348–360. [[CrossRef](#)]
18. Lei, X.; Hu, H.; Wu, W.; Liu, H.; Liu, L.; Yang, W.; Zhou, Z.; Ren, W. Seed Motion Characteristics and Seeding Performance of a Centralized Seed Metering System for Rapeseed Investigated by DEM Simulation and Bench Testing. *Biosyst. Eng.* **2021**, *203*, 22–33. [[CrossRef](#)]
19. Gao, X.; Cui, T.; Zhou, Z.; Yu, Y.; Xu, Y.; Zhang, D.; Song, W. DEM Study of Particle Motion in Novel High-speed Seed Metering Device. *Adv. Powder Technol.* **2021**, *32*, 1438–1449. [[CrossRef](#)]
20. Coetzee, C.J.; Lombard, S.G. The destemming of grapes: Experiments and discrete element modelling. *Biosyst. Eng.* **2013**, *114*, 232–248. [[CrossRef](#)]
21. Ma, Z.; Li, Y.; Xu, L. Discrete-element method simulation of agricultural particles' motion in variable-amplitude screen box. *Comput. Electron. Agric.* **2015**, *118*, 92–99. [[CrossRef](#)]
22. Yu, Y.; Fu, H.; Yu, J. DEM-based simulation of the corn threshing process. *Adv. Powder Technol.* **2015**, *26*, 1400–1409. [[CrossRef](#)]
23. Liang, Z.; Li, Y.; Xu, L.; Zhao, Z. Sensor for monitoring rice grain sieve losses in combine harvesters. *Biosyst. Eng.* **2016**, *147*, 51–66. [[CrossRef](#)]
24. Romuli, S.; Karaj, S.; Müller, J. Discrete element method simulation of the hulling process of *Jatropha curcas* L. fruits. *Biosyst. Eng.* **2017**, *155*, 55–67. [[CrossRef](#)]

25. Liang, Z.; Xu, L.; De Baerdemaeker, J.; Li, Y.; Saeys, W. Optimisation of a multi-duct cleaning device for rice combine harvesters utilising CFD and experiments. *Biosyst. Eng.* **2020**, *190*, 25–40. [[CrossRef](#)]
26. Ye, G.-Y.; Xu, K.-J.; Wu, W.-K. Standard deviation based acoustic emission signal analysis for detecting valve internal leakage. *Sens. Actuators A Phys.* **2018**, *283*, 340–347. [[CrossRef](#)]
27. Thukral, A.K.; Bhardwaj, R.; Kumar, V.; Sharma, A. New Indices Regarding the Dominance and Diversity of Communities, Derived from Sample Variance and Standard Deviation. *Heliyon* **2019**, *5*, e02606. [[CrossRef](#)] [[PubMed](#)]